IEEE Photonics Journal
An IEEE Photonics Society Publication

Open Access

Optical Isolator for TE Polarized Light Realized by Adhesive Bonding of Ce:YIG on Silicon-on-Insulator Waveguide Circuits

Volume 5, Number 3, June 2013

S. Ghosh, Member, IEEE
S. Keyvaninia, Member, IEEE
Y. Shirato
T. Mizumoto, Fellow, IEEE
G. Roelkens, Member, IEEE
R. Baets, Fellow, IEEE

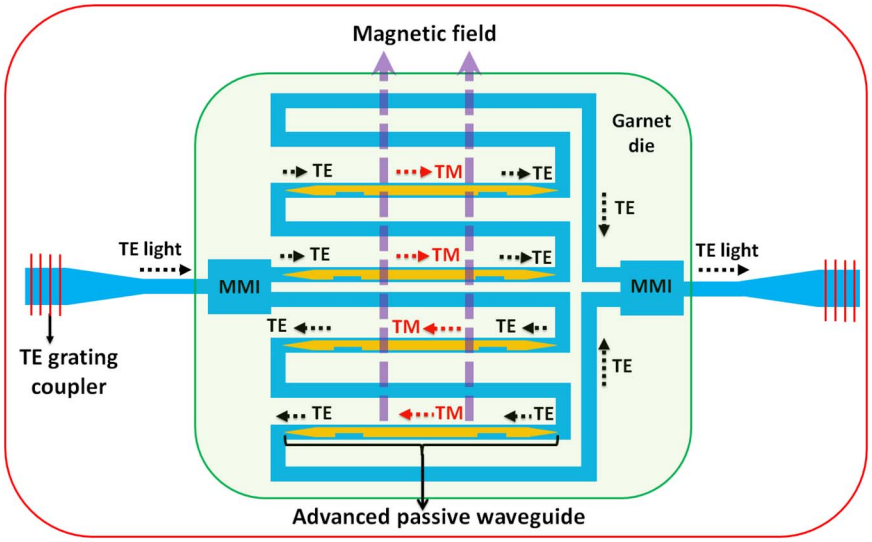

DOI: 10.1109/JPHOT.2013.2264275
1943-0655/$31.00 ©2013 IEEE

IEEE photonics SOCIETY

IEEE

Optical Isolator for TE Polarized Light Realized by Adhesive Bonding of Ce:YIG on Silicon-on-Insulator Waveguide Circuits

S. Ghosh,[1,2] ***Member, IEEE*****, S. Keyvaninia,**[1,2] ***Member, IEEE*****, Y. Shirato,**[3] **T. Mizumoto,**[3] ***Fellow, IEEE*****, G. Roelkens,**[1,2] ***Member, IEEE*****, and R. Baets,**[1,2] ***Fellow, IEEE***

[1]Photonics Research Group, Department of Information Technology, Ghent University-IMEC, 9000 Ghent, Belgium
[2]Center for Nano- and Biophotonics (NB-Photonics), Ghent University, 9000 Ghent, Belgium
[3]Department of Electrical and Electronic Engineering, Tokyo Institute of Technology, Tokyo 152-8552, Japan

DOI: 10.1109/JPHOT.2013.2264275
1943-0655/$31.00 ©2013 IEEE

Manuscript received February 28, 2013; revised May 8, 2013; accepted May 12, 2013. Date of publication May 20, 2013; date of current version June 13, 2013. Corresponding author: S. Ghosh (e-mail: samir.ghosh@intec.ugent.be).

Abstract: An optical isolator for transverse electric (TE) polarized light is demonstrated by adhesive bonding of a ferrimagnetic garnet die on top of a 380 nm thick silicon waveguide circuit. Polarization rotators are implemented in the arms of a nonreciprocal Mach–Zehnder interferometer to rotate the polarization to transverse magnetic in the nonreciprocal phase shifter regions. Calculation of the nonreciprocal phase shift (NRPS) as a function of bonding layer thickness experienced by the TM mode in the interferometer arms is presented, together with the simulation of the robustness of the polarization rotator. Experimentally, 32 dB isolation is measured at 1540.5 nm wavelength using a magnetic field transverse to the light propagation directions. This paves the way to the cointegration of laser diodes and optical isolators on a silicon photonics platform.

Index Terms: Optical isolation, photonic integration.

1. Introduction

Semiconductor laser diodes are key components in optical communication systems. The performance of such lasers can however be compromised by spurious back-reflections into the laser cavity from various parts of the optical circuit or link. The use of optical isolators can circumvent this back-reflection in the laser cavity. Besides for use in combination with discrete opto-electronic devices, the need for isolators on photonic integrated circuits is becoming of key importance, given the trend of continuous miniaturization and increasing complexity of photonic integrated transmitters. To introduce optical isolation, a nonreciprocal medium such as a magneto-optical (MO) material is required. When an electromagnetic wave propagates through a magneto-optic material, time-reversal symmetry does not hold anymore, and as a consequence, the transmission in the forward direction differs from that in the backward direction. Many approaches have been proposed for integrating such magnetic materials on waveguide platforms. Most of the conventional MO materials like cerium-doped yttrium iron garnet (Ce:YIG) and bismuth-doped yttrium iron garnet (Bi:YIG) having a high Faraday rotation coefficient in combination with low optical absorption in telecom wavelengths are difficult to deposit on semiconductor waveguide platforms. Since silicon-on-insulator (SOI) is becoming an important platform for photonic integrated circuits,

integrating such MO materials on this platform is however of key importance. There are two approaches already demonstrated for integrating MO materials on SOI. One of them is by die-to-wafer bonding [1], [2], and another one is using pulsed laser deposition or magnetron sputtering deposition [3]–[6] of MO materials on top of silicon waveguide circuits. The deposition of MO materials on SOI leads to various issues like cracking during rapid thermal annealing (RTA) due to the thermal expansion coefficient mismatch, the deterioration of MO properties, high insertion losses due to scattering, etc. The material properties and the integration issues have already improved to some extent by defining an ultrathin layer of the respective magnetic material on the semiconductor substrate, which is then annealed, after which a relatively thick layer can be further grown on top of the seed layer [6]. The direct molecular bonding of MO materials on silicon waveguide circuits is another approach [7]–[10], but this approach demands atomically smooth surfaces for high bonding yield. Another elegant bonding method is the adhesive DVS-benzocyclobutene (BCB) bonding technique that is recently reported [11], [12], which relaxes the requirements regarding surface roughness for a strong bond. Apart from these two approaches, several nonmagnetic approaches are also proposed mainly based on photonic transitions [13]–[15] and nonlinear optical processes [16], [17]. However, in these structures, optical isolation occurs either only in specific power ranges or with either associated modulation sidebands or substantial intrinsic loss. Most semiconductor lasers emit transverse electric (TE) polarized light. To protect these devices from back-reflections, an optical isolator operating in TE mode is required instead of the regular TM polarization operation mode. In this paper, a planar-waveguide-based polarization rotator is implemented to achieve the required polarization rotation. A SOI Mach–Zehnder interferometer (MZI) consisting of such polarization rotators in both arms is designed to realize an optical isolator for TE polarized light. A die of Ce:YIG is adhesively bonded on top of the 380 nm thick silicon waveguide circuit using BCB. This 380 nm waveguide layer thickness is perfectly suited for the heterogeneous integration of III–V on silicon single wavelength lasers as was recently demonstrated [18]; thereby, this demonstration paves the way to the cointegration of III–V lasers and isolators on a silicon waveguide platform.

2. Device Design and Simulation

Commercial isolators are based on nonreciprocal polarization rotation of the incident light in a magneto-optic material due to the presence of a magnetic field aligned with the light propagation direction. Typically, yttrium iron garnet (YIG) is used as the Faraday rotator medium. Such a scheme is difficult to implement for waveguide-based isolators, especially on high-index contrast waveguide platforms, because of the stringent requirement on the phase matching of TE and TM modes. The device presented in this paper works on the basis of the nonreciprocal phase shift (NRPS) experienced by the TM mode propagating through the waveguide. A detailed theoretical formulation regarding the NRPS introduced by a magnetic field transverse to the light propagation direction can be found in [11] and [19]. The proposed MZI-type isolator design consists of several components such as a polarization rotator, a 380 nm thick silicon waveguide covered with Ce:YIG used as a nonreciprocal phase shifter, spot size converters between 220 nm thick silicon and 380 nm thick silicon waveguides, multimode interferometers (MMIs), and fiber-to-chip grating couplers for TE polarization [20]. A schematic of the proposed idea is shown in Fig. 1. We will call the combination consisting of two polarization rotators, two spot size converters and one nonreciprocal phase shifter of the MZI an advanced passive (ADP) waveguide section as indicated in Fig. 1. An enlarged view of such an ADP section is presented in Fig. 2, which shows all the aforementioned subcomponents. The width of the nonreciprocal phase shifter rib waveguide is designed as 600 nm to reduce the insertion loss, and it is connected to 280 nm wide waveguides at both ends by 30 μm long linear tapers. In this narrow waveguide section the polarization rotators are implemented as will be discussed later. The total size of the optical isolator is about 6 mm $\times$ 0.2 mm, whereas the total length of the nonreciprocal phase shifter is 4 $\times$ 2.86 mm (2 $\times$ 2.86 mm in each arm). The principle of operation of the device as an isolator is as follows. TE polarized light is injected using a grating coupler and is then split using a 3 dB MMI coupler, taking two different paths through the MZI arms. Let us consider the propagation through

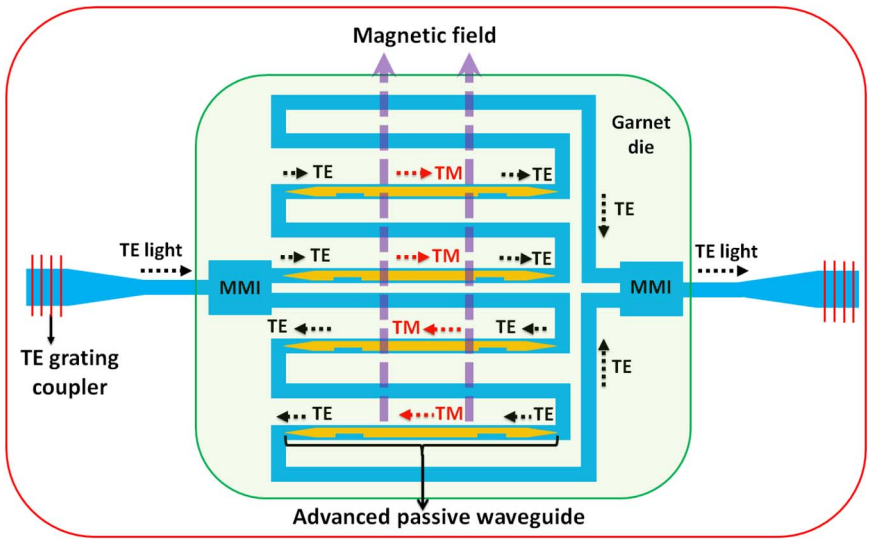

Fig. 1. Schematic of the isolator design.

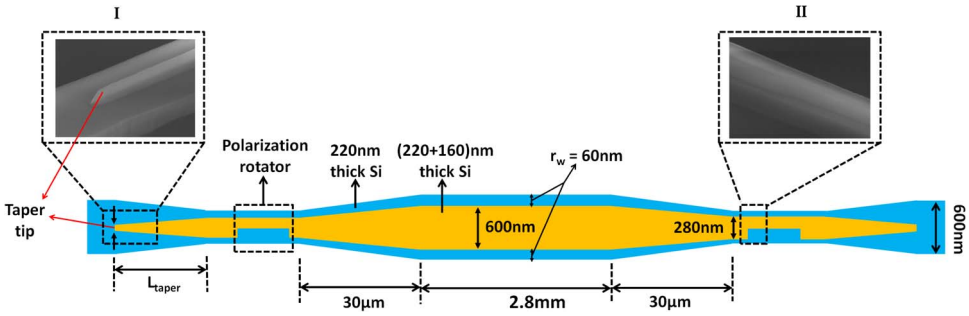

Fig. 2. Enlarged sketch of an advance passive waveguide containing two spotsize converters, two polarization rotators and a nonreciprocal phase shifter. SEM pictures in inset (I) the taper tip of the spotsize converter, inset (II) the transition section between symmetrical and asymmetrical sections of polarization rotator.

any one arm of the MZI under the presence of a transverse magnetic field. TE polarized light at the input of an ADP section is rotated to TM polarization and experiences a NRPS due to the Ce:YIG present on top of the silicon waveguide circuit and the presence of a transverse external magnetic field. After passing through the second polarization rotator in the same ADP section, the polarization is again rotated to TE and the waveguide can loop back without experiencing any NRPS. This process keeps on repeating for other ADP sections of the same arm. Finally, TE polarized light from both arms is combined at the second MMI and collected using the TE polarization grating coupler. The ADP sections are placed in both arms of the MZI in such a way that the device works in a push–pull manner when a unidirectional magnetic field is applied transverse to the light propagation. The NRPS in the ADP sections is simulated as a function of BCB thickness (t_{BCB}) at 1540 nm wavelength by the finite difference method (FDM), using the method described in [12]. The Faraday rotation coefficient (θ_F) of Ce:YIG used in the simulation is 4500 $^\circ/$cm. The thickness of the epitaxial grown Ce:YIG layer on a substituted gadolinium gallium garnet (SGGG) substrate is 300 nm. The corresponding results are presented in Fig. 3(a) for the waveguide cross-section as shown in Fig. 3(b).

Since the performance of the device mostly depends on the efficiency of the polarization rotator, a detailed discussion on its design and simulation is presented. Numerous approaches have been reported recently for realizing integrated polarization rotators. One approach is based on mode

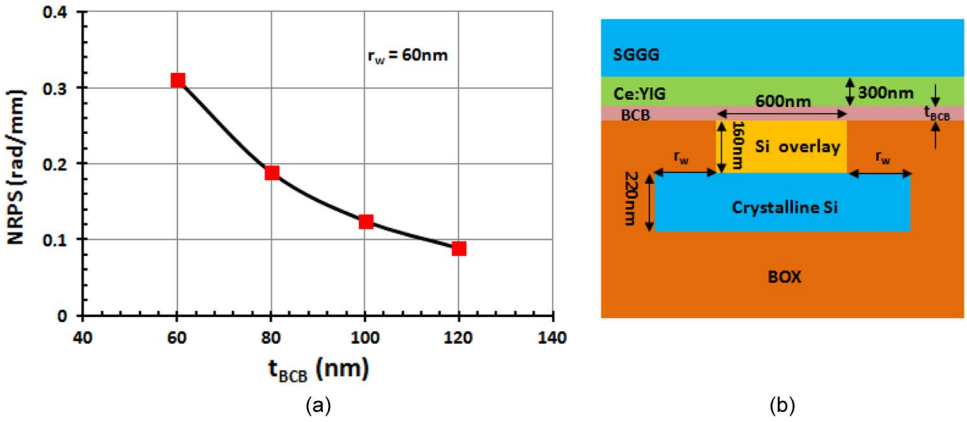

Fig. 3. (a) NRPS as a function of BCB thickness (t_{BCB}). (b) Waveguide cross-section of nonreciprocal phase shifter.

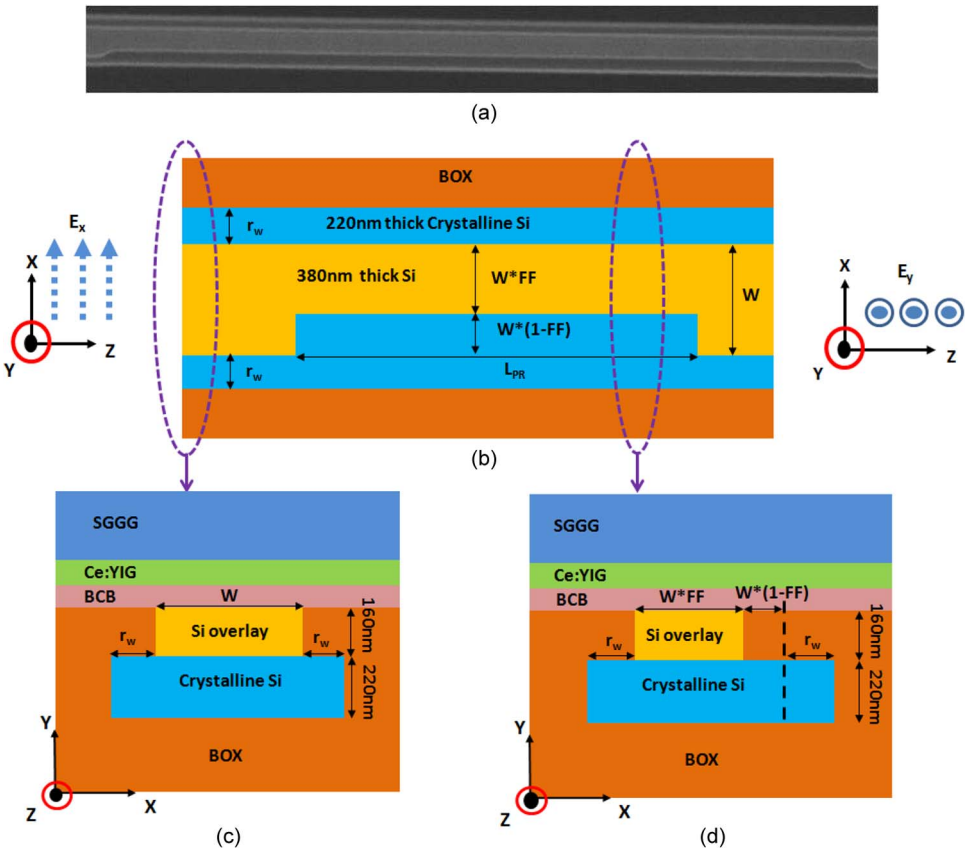

Fig. 4. (a) SEM image of the fabricated air clad polarization rotator. (b) Top view of the implemented polarization rotator. Schematic cross-sections of the symmetrical (c) and asymmetrical (d) waveguide sections.

evolution by twisted tapering of a 400 nm thick 200 nm wide silicon waveguide to a 200 nm thick 400 nm wide silicon waveguide [21]. Due to the complex geometries of the waveguide structures, this approach is not straightforward to implement. Another approach is the use of an asymmetrical directional coupler based splitter–rotator [22]. In this approach, TM and TE polarized light are separated and also rotated at the cost of longer device length and the need for a vertical

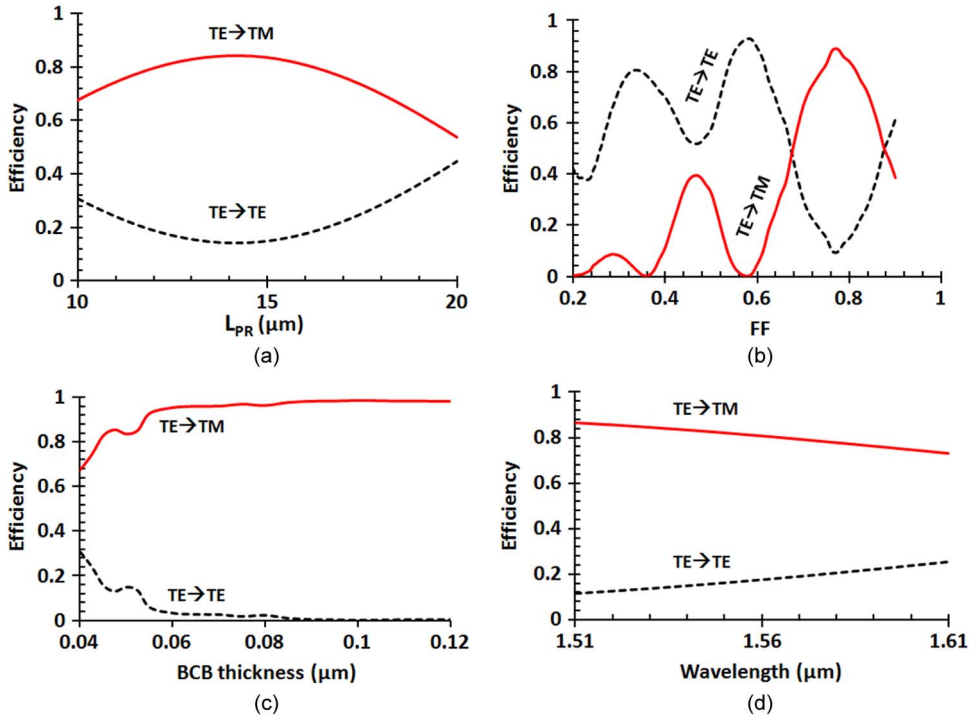

Fig. 5. Normalized efficiency as a function of (a) L_{PR} at 1.54 μm wavelength, 50 nm BCB thickness, FF = 0.8, W = 280 nm. (b) Influence of the FF on the polarization rotation efficiency at 1.54 μm wavelength, BCB thickness = 50 nm, L_{PR} = 15 μm, W = 280 nm. (c) Influence of the BCB thickness on the polarization rotation efficiency at 1.54 μm wavelength, L_{PR} = 15 μm, FF = 0.8, W = 280 nm, and (d) wavelength dependence of the polarization rotation efficiency for L_{PR} = 15 μm, BCB thickness = 50 nm, W = 280 nm, FF = 0.8.

asymmetrical structure. In the past, the use of angled sidewall waveguides was demonstrated to break vertical symmetry for polarization rotation, but it suffers from complicated fabrication steps [23]. So, less complex geometries and simple fabrication steps are highly desirable to obtain a polarization rotator. The polarization rotator implemented in this paper is based on symmetry breaking by a Si-overlay similar to the recently demonstrated work [24] except the top cladding in this case is BCB and Ce:YIG. A top view and a cross-section of the symmetrical and asymmetrical waveguide structures used in the polarization rotator are depicted in Fig. 4. W is the width of the 160 nm thick silicon overlay on top of the 220 nm thick crystalline silicon layer that is 400 nm wide. In the asymmetrical section the Si-overlay width is reduced to W $\times$ FF, where FF is the fill factor, which determines the hybrid nature of the optical modes in the asymmetrical waveguide section. To achieve the shortest length for 100% polarization rotation, the asymmetric waveguide should support modes with an eigenaxis rotated 45° with respect to the wafer surface. r_w is designed as 60 nm for this particular rotator. The cross-sectional views of both the waveguides are shown in Fig. 4(c) and (d). L_{PR} is the length of asymmetrical waveguide section, which gives optimal polarization rotation. The efficiency of the polarization rotator as a function of various parameters is presented in Fig. 5(a)–(d).

The red and dotted black curves in Fig. 5(a)–(d) correspond to the power transfer to the TM and TE polarization in the output waveguide, respectively, when the TE polarized mode is launched. From Fig. 5(b), we can see that the efficiency of the polarization rotator critically depends on the FF for a given width W.

The length L_{taper} of the spotsize converter is designed as 40 μm with a tip width of 100 nm at the interface between the 220 nm thick Si waveguide and 380 nm thick Si waveguide for optimal performance. The 1 $\times$ 2 MMIs are designed in the 220 nm waveguide layer with BCB and Garnet as top cladding. The length and width of the MMI is 6.64 μm and 2.8 μm, respectively, and there is an

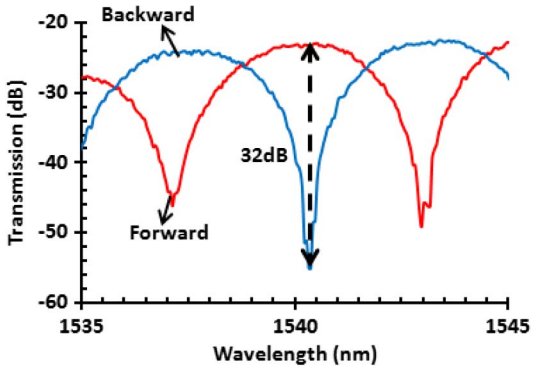

Fig. 6. Measured transmission spectra in the presence of external magnetic field.

offset of 820 nm between the output waveguides for maximum efficiency. Both the input and output waveguides have a width of 600 nm.

3. Fabrication Procedure

The SOI circuit is fabricated in a CMOS pilot line with 193 nm deep ultraviolet (DUV) lithography. The SOI wafer used consists of a 220 nm thick crystalline silicon layer on top of a 2 μm thick buried oxide. In this paper, the 160 nm thick silicon overlay is polycrystalline silicon. This is achieved by sheet deposition of 160 nm thick amorphous silicon and selective removal by dry etching where required. In the exposed 220 nm waveguide layer, 70 nm deep etching allowed the realization of the grating couplers, while a complete 220 nm deep etch defines the strip waveguides. In the final step, the amorphous silicon is annealed to transform it to polycrystalline silicon. Fig. 1 depicts that only the ADP waveguide sections of the MZI arms have a poly Si overlay. In principle, the poly crystalline silicon can be substituted by crystalline silicon, which results in lower loss; however, this process was not available at the time of fabrication. After SOI wafer fabrication, a 4 mm $\times$ 4 mm garnet die containing Ce:YIG on SGGG is bonded on top of the SOI using BCB. In this process, the SOI is cleaned by a standard SC-1 cleaning method (15 minutes in a solution of deionized water: H_2O_2 : $NH_4OH = 5 : 1 : 1$ at 70 °C–80 °C), after which it is rinsed and dried at 150 °C. Mesithylene-diluted BCB (Mesithylene: BCB $= 3 : 1$) is spin coated onto the SOI at 3000 rotation per minute for 40 seconds. In this device demonstration, the trenches of the silicon waveguide were not filled by SiO_2 prior to bonding to achieve a planarized bonding surface; rather, the trenches were filled by BCB after spin coating. Since the refractive index of BCB (1.54) is very similar to that of SiO_2 (1.45) the performance of the polarization rotator is not affected. The BCB coated SOI is kept at 150 °C for 10 minutes prior to bonding to evaporate the mesitylene so that only a thin layer of BCB remains on top of the SOI. Meanwhile, the garnet die is also cleaned by acetone and iso-propylalcohol (IPA), and it is placed on top of the SOI waveguide circuit, after which it is cured.

4. Measurement Results

TE polarized light from a tunable laser is injected and collected by grating couplers at the ends of the MZI. An external magnetic field transverse to the light propagation is applied with the aid of a miniature Nd–Fe–B magnets stack placed on top of the garnet die. Forward and backward transmission curves are obtained by switching optical input and output fibers during the measurements while keeping the magnetic field unaltered. The prototype device discussed in this paper is designed to be optically narrow band to easily observe the isolation behavior, by introducing a path length difference between both arms of the interferometer. The measured transmission spectra for forward and backward directions are presented in Fig. 6. An isolation of 32 dB is measured at wavelength of 1540.5 nm. The NRPS is 0.27 rad/mm calculated from the measured transmission spectra in Fig. 6, which implies that the BCB thickness between the Ce:YIG and silicon is between 50 nm and 60 nm. The insertion loss of the device is 22 dB at the maximum isolation point. A

TABLE 1

SOI based magneto-optical isolators

Research Group	Device type	Fabrication technique	Isolation	Insertion loss
Ghent University (This work)	MZI	BCB bonding	32 dB	22 dB
Ghent University [11]	MZI	BCB bonding	25 dB	14 dB
Ghent University [12]	MZI	BCB bonding	11 dB	14 dB
Tokyo Institute of Technology [7]	MZI	Direct molecular bonding	21 dB	8 dB
Tokyo Institute of Technology [9]	MZI	Direct molecular bonding	18 dB	6 dB
UCSB [8]	Ring	Direct molecular bonding	9 dB	-
MIT [6]	Ring	Pulsed laser deposition	19.5 dB	20 dB

performance based comparison between all the demonstrated optical isolators integrated on a silicon platform is presented in Table 1. The exact breakdown of the insertion loss is difficult to assess based on the fabricated devices but can for a large part be attributed to the scattering losses in the poly Si (20 dB/cm) and in the Ce:YIG (30 dB/cm). Therefore, switching to c-Si overlay and improving the Ce:YIG deposition process are keys to reduce the insertion loss of the device.

5. Conclusion

In this paper, a novel optical isolator based on integrated polarization rotators for TE polarized light integrated on a 380 nm thick silicon-on-insulator waveguide platform is presented. A maximum isolation of 32 dB is obtained experimentally at 1540.5 nm wavelength. This demonstration provides a path toward the direct heterogeneous integration of optical isolators and laser diodes (TE-emitting) on a silicon platform. While the measured isolation of 32 dB is to our knowledge a record on silicon platform, improvements in the device insertion loss need to be made to make this a viable approach. This is mainly related to a reduction in material scattering losses.

Acknowledgment

The authors would like to acknowledge helps from several people as E. Lambert and S. Pathak for helping in optical mask design, D. Vermeulen for assisting in simulations for the polarization rotator and L. Van Landschoot for SEM images.

References

[1] G. Roelkens, J. Brouckaert, D. Van Thourhout, R. Baets, R. Notzel, and M. Smit, "Adhesive bonding of InP/InGaAsP dies to processed silicon-on-insulator wafers using DVS-bis-benzocyclobutene," *J. Electrochem. Soc.*, vol. 153, no. 12, pp. G1015–G1019, 2006.

[2] S. Keyvaninia, M. Muneeb, S. Stankovic, P. J. Van Veldhoven, D. Van Thourhout, and G. Roelkens, "Ultra-thin DVS-BCB adhesive bonding of III–V wafers, dies and multiple dies to a patterned silicon-on-insulator substrate," *Opt. Mater. Exp.*, vol. 3, no. 1, pp. 35–46, Jan. 2013.

[3] S. Y. Sung, X. Qi, and B. J. H. Stadler, "Integrating yttrium iron garnet onto nongarnet substrates with faster deposition rates and high reliability," *Appl. Phys. Lett.*, vol. 87, no. 12, pp. 121111-1–121111-3, Sep. 2005.

[4] M. B. Park and N. H. Cho, "Structural and magnetic characteristics of yttrium iron garnet (YIG,Ce:YIG) films prepared by RF magnetron sputter techniques," *J. Magn. Magn. Mater.*, vol. 231, no. 2, pp. 253–264, Jun. 2001.

[5] S. Higuchi, K. Ueda, F. Yahiro, Y. Nakata, H. Uetsuhara, T. Okada, and M. Maeda, "Fabrications of cerium-substituted YIG thin films for magnetic field sensor by pulsed-laser deposition," *IEEE Trans. Magn.*, vol. 37, no. 4, pp. 2451–2453, Jul. 2001.

[6] L. Bi, J. Hu, P. Jiang, D. H. Kim, G. F. Dionne, L. C. Kimmerling, and C. A. Ross, "On-chip optical isolation in monolithically integrated nonreciprocal optical resonators," *Nat. Photon.*, vol. 5, no. 12, pp. 758–762, 2011.

[7] Y. Shoji, T. Mizumoto, H. Yokoi, I.-W. Hsieh, and R. M. Osgood, Jr., "Magneto-optical isolator with silicon waveguides fabricated by direct bonding," *Appl. Phys. Lett.*, vol. 92, no. 7, pp. 071117-1–071117-3, Feb. 2008.

[8] M. C. Tien, T. Mizumoto, P. Pintus, H. Kromer, and J. E. Bowers, "Silicon ring isolator with bonded nonreciprocal magneto-optic garnets," *Opt. Exp.*, vol. 19, no. 12, pp. 11 740–11 745, Jun. 2011.

[9] Y. Shoji, M. Ito, Y. Shirato, and T. Mizumoto, "MZI optical isolator with Si-wire waveguides by surface-activated direct bonding," *Opt. Exp.*, vol. 20, no. 16, pp. 18 440–18 448, Jul. 2012.

[10] T. Mizumoto, Y. Shoji, and R. Takei, "Direct wafer bonding and its application to waveguide optical isolator," *Materials*, vol. 5, no. 5, pp. 985–1004, May 2012.

[11] S. Ghosh, S. Keyvaninia, W. Van. Roy, T. Mizumoto, G. Roelkens, and R. Baets, "Ce:YIG/Silicon-on-Insulator waveguide optical isolator realized by adhesive bonding," *Opt. Exp.*, vol. 20, no. 2, pp. 1839–1848, Jan. 2012.
[12] S. Ghosh, S. Keyvaninia, W. Van Roy, T. Mizumoto, G. Roelkens, and R. Baets, "Compact Mach–Zehnder interferometer Ce:YIG/SOI optical isolators," *IEEE Photon. Technol. Lett.*, vol. 24, no. 18, pp. 1653–1656, Sep. 2012.
[13] Z. Yu and S. Fan, "Integrated non-magnetic optical isolators based on photonic transitions," *IEEE J. Sel. Topics Quantum Electron.*, vol. 16, no. 2, pp. 459–466, Mar./Apr. 2010.
[14] Z. Yu and S. Fan, "Optical isolation: A non-magnetic approach," *Nat. Photon.*, vol. 5, no. 9, pp. 517–519, 2011.
[15] H. Lira, Z. Yu, S. Fan, and M. Lipson, "Electrically driven nonreciprocity induced by interband photonic transition on a silicon chip," *Phys. Rev. Lett.*, vol. 109, no. 3, pp. 033901-1–033901-5, Jul. 2012.
[16] M. Soljaèi, C. Luo, J. D. Joannopoulos, and S. Fan, "Nonlinear photonic crystal microdevices for optical integration," *Opt. Lett.*, vol. 28, no. 8, pp. 637–639, Apr. 2003.
[17] K. Gallo, G. Assanto, K. R. Parameswaran, and M. M. Fejer, "All-optical diode in a periodically poled lithium niobate waveguide," *Appl. Phys. Lett.*, vol. 79, no. 3, pp. 314–316, Jul. 2001.
[18] S. Keyvaninia, G. Roelkens, D. Van Thourhout, C. Jany, M. Lamponi, A. L. Liepvre, F. Lelarge, D. Make, G. H. Duan, D. Bordel, and J. M. Fedeli, "Demonstration of a heterogeneously integrated III–V/SOI single wavelength tunable laser," *Opt. Exp.*, vol. 21, no. 3, pp. 3784–3792, Feb. 2013.
[19] K. Postava, M. Vanwolleghem, D. Van Thourhout, R. Baets, S. Visnovsky, P. Beauvillain, and J. Pistora, "Modeling of a novel InP-based monolithically integrated magneto-optical waveguide isolator," *J. Opt. Soc. Amer. B*, vol. 22, no. 1, pp. 261–273, Jan. 2005.
[20] D. Taillaert, P. Bienstman, and R. Baets, "Compact efficient broadband grating coupler for silicon-on-insulator waveguides," *Opt. Lett.*, vol. 29, no. 23, pp. 2749–2751, Dec. 2004.
[21] J. Zhang, M. Yu, G.-Q. Lo, and D.-L. Kwong, "Silicon-waveguide-based mode evolution polarization rotator," *IEEE J. Sel. Topics Quantum Electron.*, vol. 16, no. 1, pp. 53–60, Jan./Feb. 2010.
[22] D. Dai and J. E. Bowers, "Novel concept for ultracompact polarization splitter–rotator based on silicon nanowires," *Opt. Exp.*, vol. 19, no. 11, pp. 10 940–10 949, May 2011.
[23] C. Brooks, P. E. Jessop, H. Deng, D. O. Yevick, and G. Tarr, "Passive silicon-on-insulator polarization-rotating waveguides," *Opt. Eng.*, vol. 45, no. 4, p. 044603, Apr. 2006.
[24] D. Vermeulen, S. Selvaraja, P. Verheyen, P. Absil, W. Bogaerts, D. Van Thourhout, and G. Roelkens, "Silicon-on-Insulator polarization rotator based on a symmetry breaking silicon overlay," *IEEE Photon. Technol. Lett.*, vol. 24, no. 6, pp. 482–484, Mar. 2012.